RESEARCH ARTICLE

Macro-
molecular
Materials and Engineering
Open Access

www.mame-journal.de

Mechanically Robust Shape-Memory Organohydrogels Based on Silk Fibroin with Organogel Microinclusions of Various Sizes

*Yahya Bas and Oguz Okay**

Organohydrogels (OHGs) are soft materials with antagonistic hydrophilic and hydrophobic domains that have great interest for many different applications. This study presents the preparation of mechanically strong OHGs with shape-memory function by incorporating semicrystalline organo-microgels within the pores of silk fibroin (SF) scaffolds. In the first step, SF cryogels with various pore diameters between 26 ± 8 and 17 ± 4 µm are synthesized by cryogelation of aqueous SF solutions at concentrations between 5 and 20 w/v%. In the second step, the pores of SF scaffolds are filled with an organogel precursor solution containing n-octadecyl acrylate (C18A), acrylic acid, *N,N'*-methylene(bis)acrylamide, and an initiator. Once the free-radical polymerization took place inside the pores, OHGs containing organo-microgels of various sizes are obtained. The incorporation of the organogel component in the cryogels generates crystalline areas due to the side-by-side packed C18 side chains. OHGs' melting temperature and crystallinity level can be varied from 42 to 54 °C and from 2 to 16%, respectively. The stiffness of OHGs increases from 5.9 ± 0.5 to 18 ± 1 MPa with increasing SF concentration from 5 to 20 w/v%, which is attributed to the decreasing pore size of the cryogels and increasing thickness of the pore walls.

1. Introduction

Throughout the evolution of creatures, organisms that were adaptable to environmental changes had a much higher chance of surviving than the healthiest or most powerful ones. The existence of both hydrophilic and hydrophobic domains in the body is one of the basic strategies of adaptable organisms giving them some unique abilities like frost tolerance and adaptive biomechanics.[1–4] Scientists have used the adaptability of biological organisms as a model to create a new class of synthetic smart materials such as organohydrogels (OHGs), soft materials with antagonistic hydrophilic and hydrophobic domains that have a great interest for many different applications.[5–9] A commonly used technique to synthesize OHGs is to disperse a hydrophobic phase in an aqueous solution to form an oil-in-water emulsion followed by gelation of the aqueous phase.[10,11] Alternatively, lyophilic or hydrophobic components are introduced into a pre-formed hydrophilic network. For instance, freeze-inhibiting compounds such as sorbitol, glycol, and glycerol were incorporated into a previously prepared alginate-based hydrogel to produce freeze-tolerant materials.[12] However, these studies mainly focus on non-freezable materials rather than their adaptation capabilities. In addition, OHGs exhibit poor mechanical properties limiting their applications.

Recently, we prepared mechanically strong OHGs with shape memory function by a two-step synthetic procedure.[13] In the first step, a macroporous hydrophilic cryogel was synthesized by cryogelation of an aqueous 5 w/v% methacrylated silk fibroin (meth-SF) solution containing N,N-dimethylacrylamide (DMAA) as a spacer in the presence of 1,4-butanediol diglycidyl ether (BDDE), and N,N,N',N'-tetramethylethylenediamine (TEMED) as a cross-linker and catalyst, respectively. The resulting cryogel, consisting of an interconnected meth-SF and poly(DMAA) network, exhibited a total pore volume of 11.5 mL g^{-1}, and an average pore diameter of 44 µm. The cryogel scaffold was then submerged into a solution containing n-octadecyl acrylate (C18A), acrylic acid (AAc), N,N'-methylene(bis)acrylamide (BAAm), and α,α'-azoisobutyronitrile (AIBN) to fill the scaffold pores with the solution of the organogel precursor. After the polymerization reactions within the pores, an OHG consisting of meth-SF/DMAA-based cryogel with organogel microinclusions was obtained. The disadvantage of this strategy is that methacrylation of silk fibroin (SF) was an additional step to obtain OHG materials, and DMAA
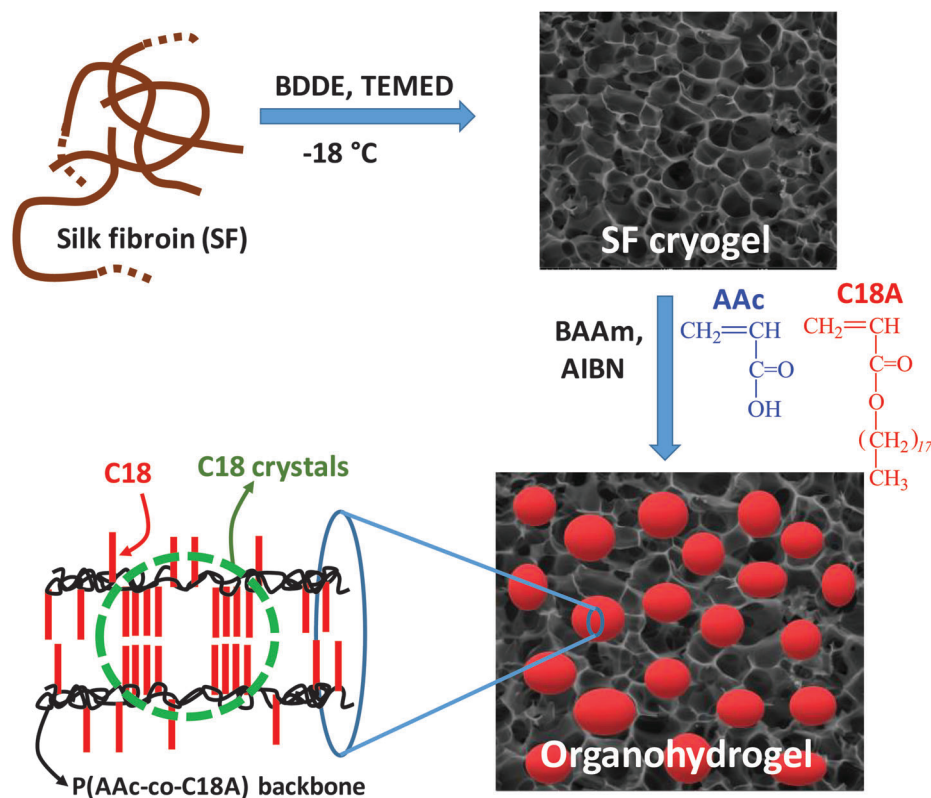
Y. Bas, O. Okay
Department of Chemistry
Istanbul Technical University
Maslak, Istanbul 34469, Turkey
E-mail: okayo@itu.edu.tr
Y. Bas
Department of Chemistry
Istanbul University
Vezneciler, Istanbul 34134, Turkey

ADVANCED
SCIENCE NEWS
www.advancedsciencenews.com

Macro-
olecular
Materials and Engineering
Open Access

www.mame-journal.de

Scheme 1. Cartoon presenting formation of shape-memory organohydrogels (OHGs) from SF cryogels by filling their pores with the organogel precursors AAc, C18A, BAAm, and the initiator AIBN followed by free-radical polymerization.

as a spacer was needed to obtain the cryogel. In addition, the size of the organogel microinclusions cannot be changed because the scaffold pores in which the organogel was synthesized have a fixed diameter.

In the present study, we use SF instead of meth-SF in the cryogel preparation so that the incorporation of DMAA units into the cryogel network is not needed. We also varied the pore diameter of the cryogels and hence, the size of organogel microinclusions by varying SF concentration between 5 and 20 w/v%. The cryogels are synthesized by cross-linking SF in aqueous solutions at −18 °C in the presence of BDDE cross-linker and TEMED catalyst (**Scheme 1**). The freeze-dried cryogels of various pore sizes are then submerged in an ethanolic solution containing C18A, AAc, BAAm, and AIBN as the hydrophobic crystallizable, and hydrophilic monomers, chemical cross-linker, and initiator, respectively. After free-radical polymerization within the pores, shape-memory OHGs containing semi-crystalline organogel microinclusions of various sizes were obtained. As will be seen below, the stiffness of OHGs increases from 5.9 ± 0.5 to 18 ± 1 MPa with increasing SF concentration from 5 to 20 w/v %, which is attributed to the decreasing pore size of the cryogels and increasing thickness of the pore walls that surround and protect the brittle organogel microinclusions from damage.

2. Results and Discussion

In the first section, we discuss the characteristics of silk fibroin (SF) cryogels synthesized at various SF concentrations.

The preparation of OHGs by filling the cryogel pores of various sizes with organo-microgels and their properties will then be discussed.

2.1. SF Cryogels

We synthesize SF cryogels from aqueous SF solutions of four different concentrations C_{SF}, namely 5, 10, 15, and 20 w/v%, using BDDE and TEMED as a cross-linker and accelerator, respectively (see Supporting Information for further details). The cryogelation reactions were carried out at −18 °C for 24 h. After the as-prepared cryogels are immersed in an excess of water at 23 ± 2°C, we determine the insoluble (gel) fraction W_g, and their mass and volume swelling ratios in water. The gel fraction W_g is 1.02 ± 0.06 revealing that SF is completely cross-linked to form a cryogel network (Figure S1, Supporting Information). We plot in **Figure 1**a the equilibrium mass (m_{rel}) and volume swelling ratios (V_{rel}) of the cryogels with respect to as-prepared state as a function of C_{SF}. Both m_{rel} and V_{rel} are around 0.9 independent of C_{SF} revealing their anti-swelling behavior when immersed in water. We also calculated the equilibrium mass q_w and volume swelling ratios q_v of the cryogels with respect to their dried states (Figure 1b). Although q_v is around unity and hence supporting the anti-swelling behavior, the mass swelling degree q_w is much larger than q_v, and the difference between q_w and q_v decreases as C_{SF} is increased.

Because q_v originates from the swelling of the pore walls while q_w also includes water locating in the pores, decreasing q_w with

ADVANCED
SCIENCE NEWS
www.advancedsciencenews.com

[M] acro-
molecular
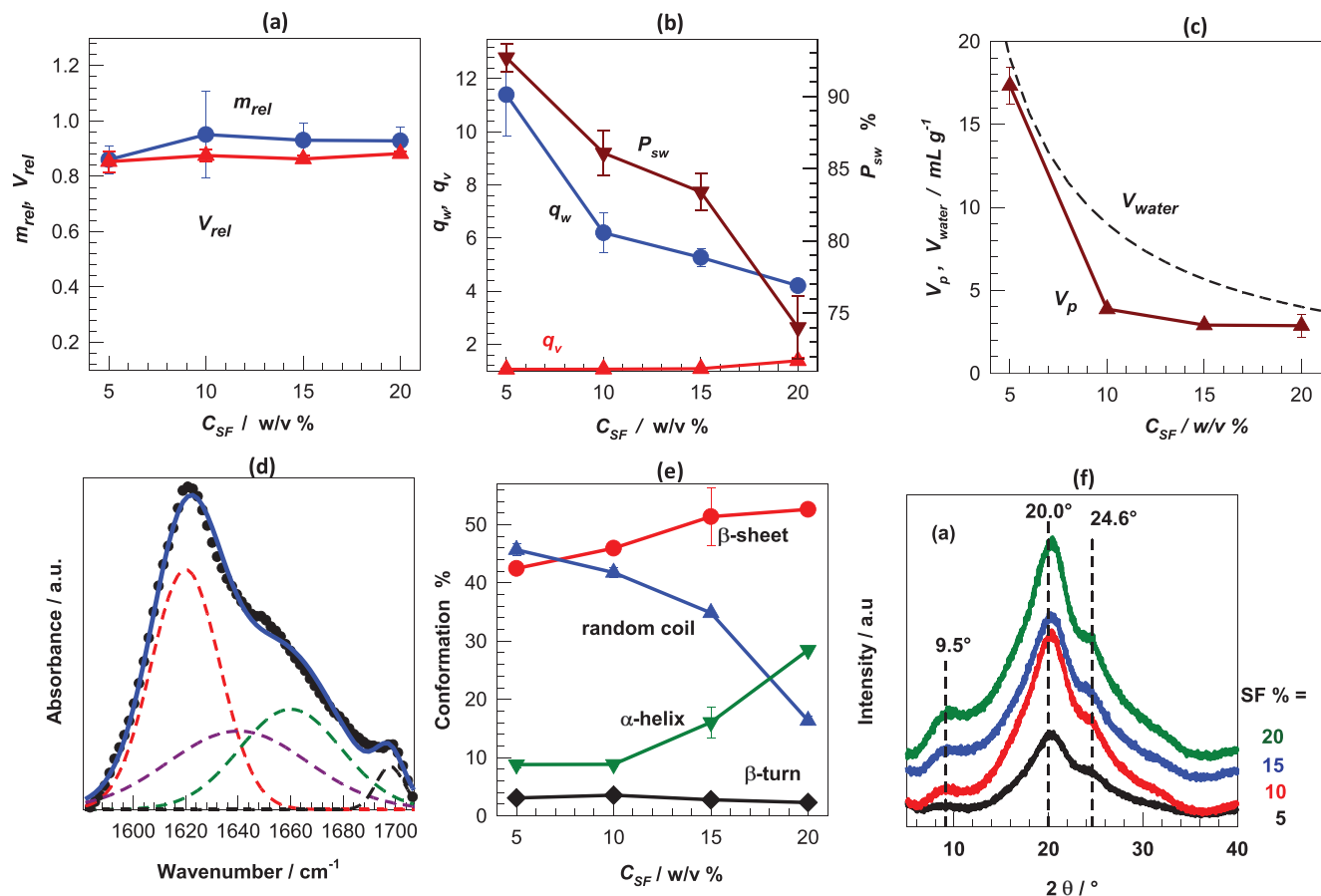Materials and Engineering
Open Access
www.mame-journal.de

Figure 1. a) The mass and volume swelling ratios, m_{rel} and V_{rel}, respectively, of SF cryogels with respect to the as-prepared state plotted against C_{SF}. b) The mass and volume swelling ratios q_w and q_v, respectively, of the same cryogels with respect to their dried states, and their porosities P_{sw} as a function of C_{SF}. c) V_p and V_{water}, plotted against C_{SF}. d) Amide I region of the FTIR spectrum for the cryogel formed at $C_{SF} = 15$ w/v%. The symbols represent the original spectrum, and the solid blue line is the best fitting curve to the spectrum. The dashed curves represent the hidden peaks at 1620, 1640, 1660, and 1698 cm^{-1}, which are typical for β-sheet, random coil, α-helix, and β-turn configurations, respectively. e) Conformation of SF in cryogels plotted against C_{SF}. f) XRD patterns of the cryogels prepared at different C_{SF} as indicated.

increasing C_{SF} suggests decreasing porosity of the cryogels.[14] Assuming equal densities of SF and water (see Supporting Information), the swollen state porosity P_{sw} is related to the swelling ratios q_w and q_v by,

$$P_{sw} = 1 - \frac{q_v}{q_w} \qquad (1)$$

Figure 1b presents the swollen state porosity P_{sw} of the cryogels plotted against C_{SF}. For comparison, the total pore volume V_p of cryogels in their dried states determined experimentally are shown in Figure 1c. It is seen that both P_{sw} and V_p decrease with increasing C_{SF}, which we attribute to the simultaneous decrease in the amount of water of the reaction system. For instance, the dashed curve in Figure 1c presents the volume of water (V_{water}) in the reaction system per gram of SF plotted against C_{SF}. Under cryogenic condition, because water turns into ice serving as a template for pores,[15,16] V_{water} represents the maximum achievable pore volume in the cryogel. Thus, the porosity of SF cryogels can be adjusted over a wide range by varying the water content of the aqueous SF solution.

The microstructure of SF cryogels is investigated by Fourier transform infrared (FTIR) and X-ray diffraction (XRD) measurements. The sol-to-gel transition in SF is known to occur with increasing content of β-sheet crystals and, this transition is facilitated by introducing chemical cross-links such as BDDE between SF molecules, reducing the chain mobility and triggering the conformational transition to β-sheet structure.[17,18] The adsorption peaks at 1620, 1640, 1660, and 1698 cm^{-1} in the Amide I region of FTIR spectra are typical for β-sheet, random coil, α-helix and β-turn configurations, respectively.[17,19,20] The ratio of conformations is determined by deconvolution of the Amide-I band of the spectra, and curve fitting of the characteristic SF peaks (Figure 1d; Figure S2, Supporting Information).[17] Calculations show that the amount of β-sheet of SF rises from 12 $\pm$ 2% to 42.5 $\pm$ 0.5% after gelation at $C_{SF} = 5$ w/v%, while it further increases to 52.6 $\pm$ 0.3% with increasing C_{SF} to 20 w/v% (Figure 1e). XRD results also support this finding (Figure 1f). The major peak at 20.0° and the two small peaks at 9.5 and 24.6° corresponding to crystalline spacing distances of 4.4, 9.3, and 3.6 Å, respectively, are typical for the β-sheet structure of SF.[17,19,20] These peaks become sharper as C_{SF} is increased revealing increasing number of

**ADVANCED
SCIENCE NEWS**

www.advancedsciencenews.com

**[M] acro-
molecular
Materials and Engineering**
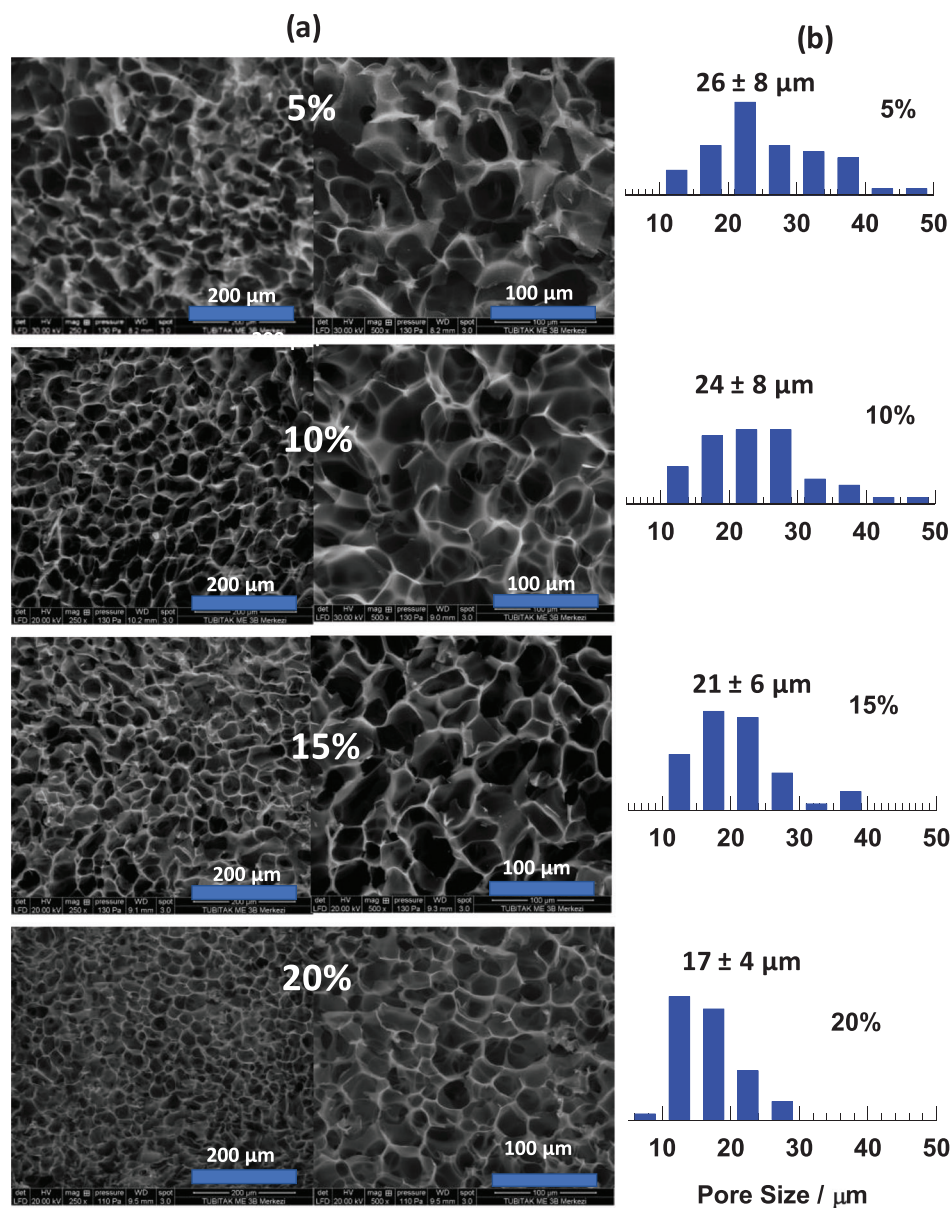Open Access

www.mame-journal.de

Figure 2. a) SEM images of the cryogel scaffolds formed at various C_{SF} as indicated. b) Pore size distribution of the cryogels. The number average pore size and standard deviations are indicated.

β-sheet crystals. The increasing β-sheet content with C_{SF} is likely due to the increasing amount of SF in the unfrozen regions during cryogelation facilitating the conformational transition to β-sheet structure.

The porous morphology of SF cryogels is studied by scanning electron microscopy (SEM). **Figure 2**a presents their SEM images at two different magnifications. All cryogels exhibit regular micrometer-sized pores with honeycomb morphology. The average pore diameter decreases while the size distribution of the pores becomes narrower as C_{SF} is increased. For instance, the average pore diameter drops from 26 ± 8 to 17 ± 4 µm, and the average thickness of the pore walls increases from 10 ± 2 to 30 ± 5 µm

as C_{SF} increases from 5 to 20 w/v% (Figure 2b; Figure S3, Supporting Information). The inverse relation between the pore size and the amount of monomer or polymer during cryogelation was also reported before for several cryogelation systems.[16,18,21–24] For instance, in polyacrylamide cryogels, the average pore diameter drops from 55 to 10 µm as the monomer concentration is increased from 3 to 30%.[21] We attribute this behavior to decreasing water content as C_{SF} is increased (Figure 1c), leading to the formation of thicker pore walls, lower porosities, and smaller pores. The inverse relation may also be attributed to the increasing volume of unfrozen microregions in the cryogelation system as the amount of SF is increases.[16]
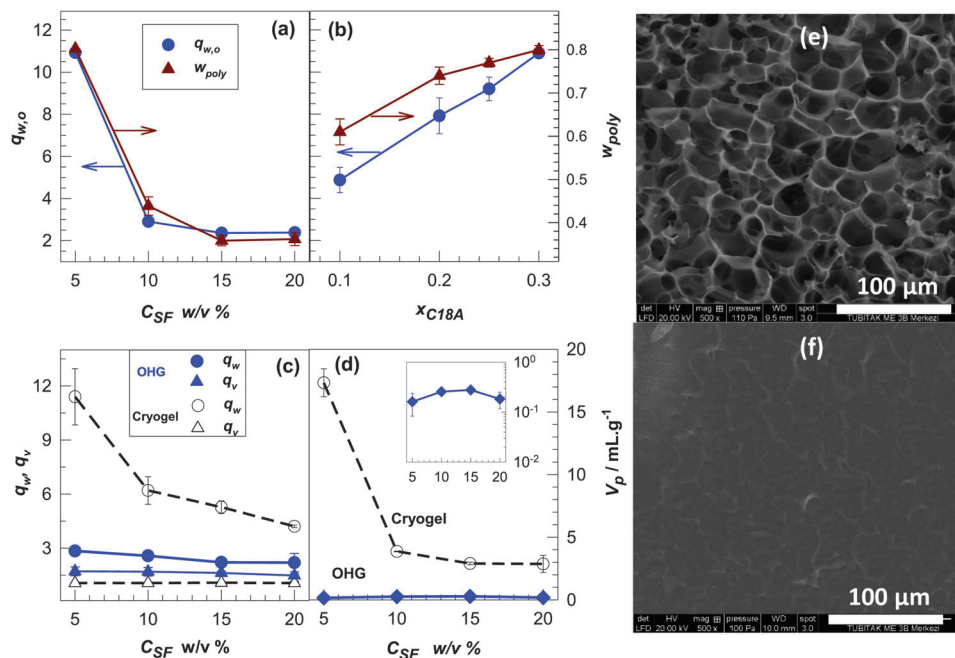
Figure 3. a,b) The swelling ratio $q_{w,o}$, and the mass fraction of AAc/C18A copolymer w_{poly} in OHGs plotted against C_{SF} and x_{C18A}, respectively. In (a), $x_{C18A} = 0.30$ while in (b), $C_{SF} = 5$ w/v%. c) The equilibrium mass q_w c) and volume swelling ratios q_v of the OHGs and cryogels plotted against C_{SF}. d) The pore volume V_p f) of the OHGs and cryogels plotted against C_{SF}. The inset shows the data of OHGs in a semi-logarithmic plot. e,f) SEM images of a cryogel specimen prepared at $C_{SF} = 20$ w/v% before e) and after polymerization at $x_{C18A} = 0.25$ (f).

2.2. SF-Based Organohydrogels

For the preparation of organohydrogels (OHGs), freeze-dried SF cryogels are first submerged into an ethanolic solution of organogel precursor consisting of C18A, AAc, BAAm, and AIBN. We fix the total monomer concentration of the solution at 41 w/v%. The concentrations of BAAm cross-linker and AIBN initiator are also fixed at 1 mol % (with respect to the monomers) while the mole fraction of C18A in the monomer mixture (x_{C18A}) is varied (see Supporting Information for further details). The scaffold specimens immediately absorbed the precursor solution during which their mass significantly increased while their volume remained unchanged, indicating that the pores were filled with the solution. After filling the pores with the solution, free-radical polymerization of the precursors is carried out within the pores of the cryogels at 50 °C for 24 h.

We carried out two sets of experiments: In the first set, SF cryogel formed at $C_{SF} = 5$ w/v % is immersed in precursor solutions of varying x_{C18A} between 0 and 0.30. In the second set, SF cryogels formed at various C_{SF} are immersed in a precursor solution with $x_{C18A} = 0.30$. Once the free-radical polymerization of the organogel precursors took place inside the pores, the OHG specimens thus formed were first immersed in an excess of ethanol, and then in water to extract the soluble species. The gel fraction W_g of OHGs was found to be around unity revealing that the monomers are completely converted into the BAAm-cross-linked AAc/C18A copolymer filling the cryogel pores. For the precursor solution, let C_o be the total monomer concentration (41 w/v %), and $q_{w,o}$ be the equilibrium mass swelling ratio of the cryogel in

the precursor solution. The mass fraction of AAc/C18A copolymer w_{poly} in OHG (on dry bases) is given by,

$$w_{poly} = \frac{(q_{w,o} - 1)\ C_o}{1 + (q_{w,o} - 1)\ C_o} \quad (2)$$

Figure 3a,b shows the mass swelling ratio $q_{w,o}$ of the cryogels in the precursor solution, and the weight fraction of AAc/C18A copolymer w_{poly} in OHGs plotted against C_{SF} and x_{C18A}, respectively. Similar to the mass swelling ratio q_w of the cryogels in water (Figure 1b), their mass swelling ratio $q_{w,o}$ in the precursor solution is very large at $C_{SF} = 5$ w/v% while it rapidly decreases with rising SF content from 5 to 10 w/v% to approach a limiting value. The copolymer content w_{poly} of OHGs varies similar to the $q_{w,o}$, and the largest amount of copolymer could be introduced in the cryogel formed at the lowest SF content due to its largest pore volume. Thus, the largest amount of organogel can be incorporated in the cryogel scaffold formed at the lowest SF content (5 w/v%), and at the highest C18A mole fraction x_{C18A}. The filled circles and triangles in Figure 3c represent the equilibrium mass q_w and volume swelling ratios q_v of OHGs in water, respectively, plotted against C_{SF}. For comparison, q_w and q_v of the starting cryogels are also given by the open circles and triangles, respectively. The volume swelling ratio q_v of OHGs slightly increases while their mass swelling ratio q_w significantly decreases as compared to those of the cryogels. The increase in q_v is attributed to the hydrophilic AAc units of the organogel while the decrease in q_w is likely due to the plugging of cryogel pores by the organogels. Indeed, both the porosity P_{sw} and total pore volume V_p significantly decrease
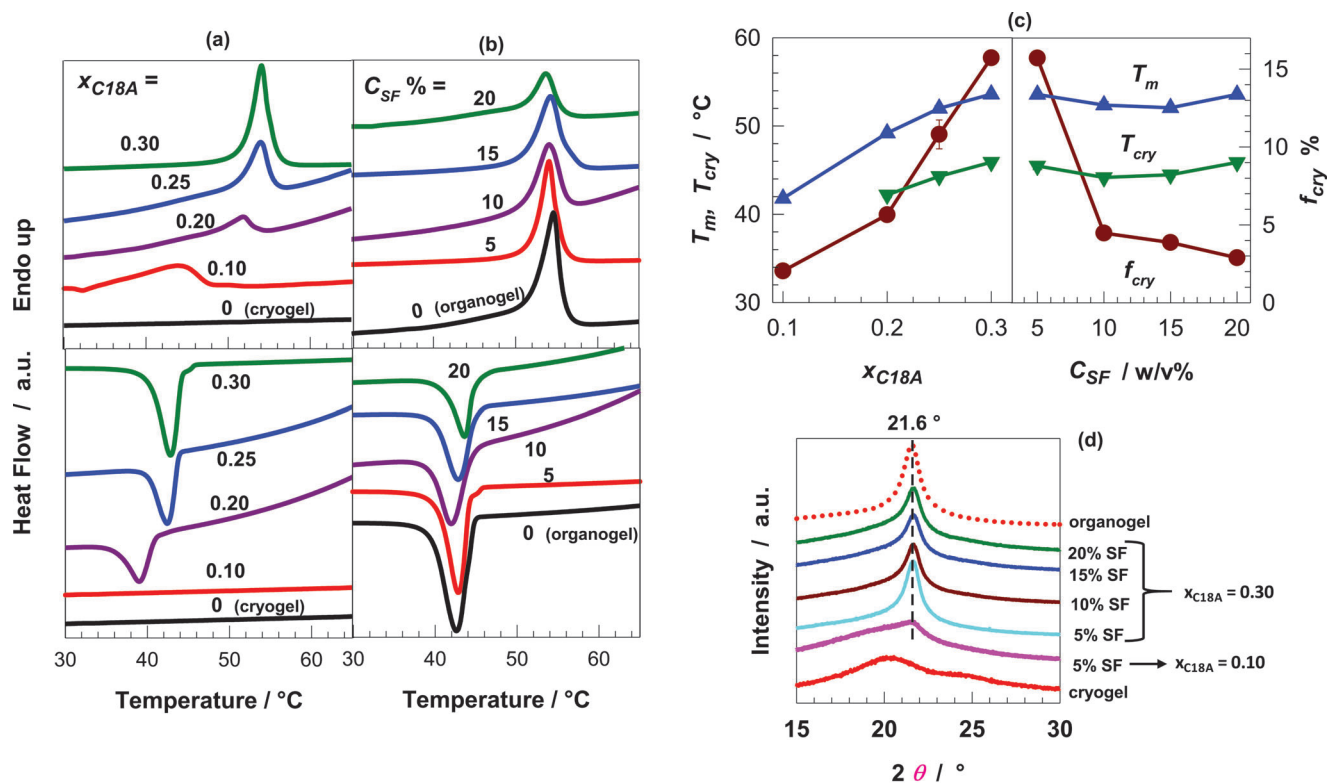
ADVANCED
SCIENCE NEWS
www.advancedsciencenews.com

{M}acro-
molecular
Materials and Engineering
Open Access
www.mame-journal.de

Figure 4. a,b) DSC scans of OHGs formed at various x_{C18A} (a) and C_{SF} (b) during a heating-cooling cycle between 30 and 70 °C. For comparison, the scans for the cryogel formed at $C_{SF} = 5$ w/v% and organogel with $x_{C18A} = 0.30$ are also shown. c) Melting T_m and crystallization temperatures T_{cry}, and the degree of crystallinity f_{cry} of OHGs shown as functions of x_{C18A} and C_{SF}. d) XRD patterns of the organogel, cryogel formed at $C_{SF} = 5$ w/v%, and OHGs at various x_{C18A} and C_{SF} as indicated.

after formation of OHGs (Figure 3d; Figure S4, Supporting Information). For instance, the pore volume V_p of the cryogel prepared at $C_{SF} = 5$ w/v% decreases from 17 ± 1 to 0.2 ± 0.1 mL g^{-1} after OHG formation at $x_{C18A} = 0.30$ (inset to Figure 3d). SEM images of the OHGs also reveal the disappearance of the pores after the polymerization reactions (Figure 3e,f).

We investigated the thermal properties of OHGs by DSC and XRD measurements. **Figure 4**a,b shows DSC scans of OHGs formed at various x_{C18A} (a) and C_{SF} (b) during a heating-cooling cycle between 30 and 70 °C. For comparison the data for the cryogel with $C_{SF} = 5$ w/v% and the organogel with $x_{C18A} = 0.30$ are also shown in the figures. The incorporation of the organogel component in the cryogels results in the appearance of a melting peak in DSC scans that becomes sharper and more intense as x_{C18A} is increased, or C_{SF} is decreased. Similar behavior also appears in the crystallization peak of OHGs except that the peak at $x_{C18A} = 0.10$ does not appear, which is likely due to the confinement of the organogel inside the pores hindering alignment of C18 side chains at low x_{C18A} values. Figure 4c presents the melting T_m and crystallization temperatures T_{cry}, and the degree of crystallinity f_{cry} of OHGs shown as functions of x_{C18A} and C_{SF}. By increasing x_{C18A}, OHG's melting temperature T_m and crystallinity level f_{cry} could be increased from 42 to 54 °C, and from 2 to 16%, respectively, due to the increasing amount of C18A units in the organogel component of OHG forming larger amount of alkyl crystals of higher stability. Moreover, increasing C_{SF} from 5 to 20% does not affect both T_m and T_{cry}, but f_{cry} significantly de-

creases from 16 to 3%. This is attributed to decreasing pore volume and pore diameter as C_{SF} is increased (Figures 1 and 2), leading to the incorporation of a smaller amount of organogel. XRD measurements also support formation of crystalline domains after incorporation of organogel microinclusions into cryogels (Figure 4d). The peak at 20° appearing for the cryogel due to the β-sheet crystalline structure is shielded by the strong peak of OHGs at 21.6° that is typical for alkyl side chains packed side by side with a spacing distance of 0.41 nm.[25,26] The intensity of the crystalline peak increases with increasing x_{C18A}, or decreasing C_{SF} as similar to the crystallinity fraction f_{cry} calculated from DSC results.

The existence of crystalline domains in OHGs resulted in the temperature dependence of their viscoelastic properties. **Figure 5**a presents the frequency dependence of the storage modulus G', loss modulus G'' and loss factor $\tan \delta$ of an OHG specimen formed at $C_{SF} = 5$ w/v% and $x_{C18A} = 0.30$. The frequency sweep tests are first conducted at 25 °C, and then after heating to 65 °C, and finally after cooling back to 25 °C. The modulus G' 10-fold decreases upon heating from 25 to 65 °C (from 2 to 0.2 MPa) while cooling back recovers the original modulus revealing reversible switchable viscoelastic behavior of OHGs. This behavior is a prerequisite for the observation of thermal induced shape-memory function. Thus, above T_m, the OHG specimen becomes weak so that it can easily be deformed into any shape, i.e., a bended shape, while cooling below T_m fixes the temporary bended shape because of the reformation of the crystalline
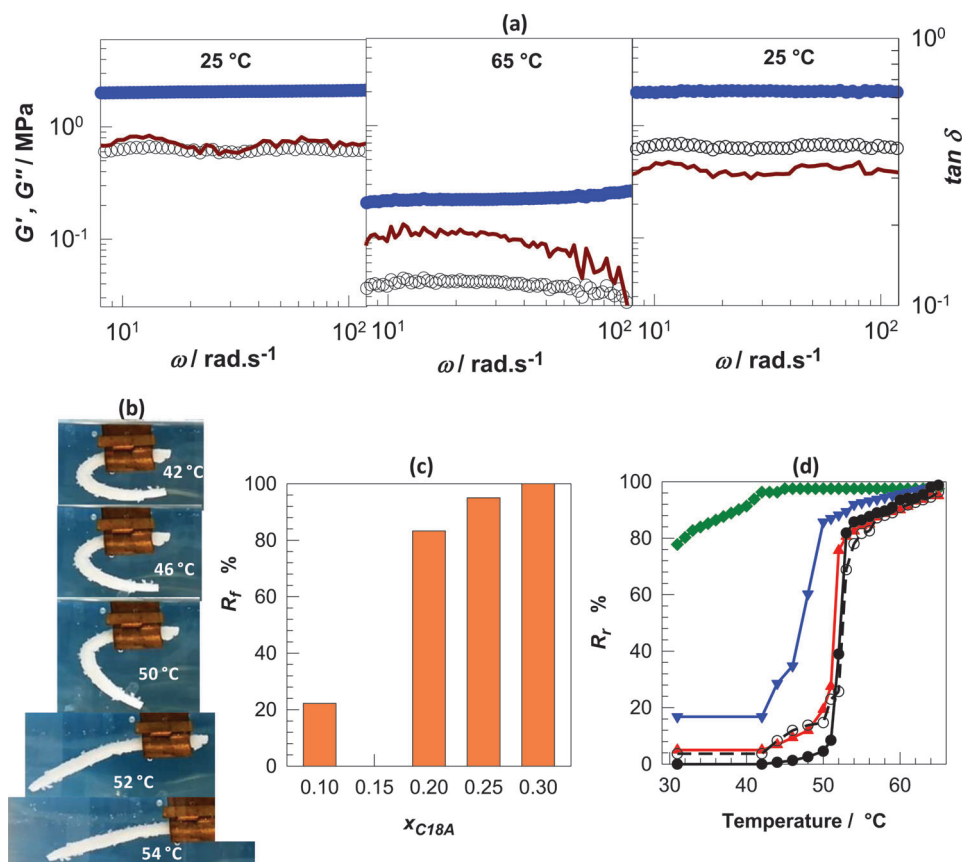
**ADVANCED
SCIENCE NEWS**

www.advancedsciencenews.com

**Macro-
olecular
Materials and Engineering**

www.mame-journal.de

Figure 5. a) Frequency (ω) sweep results of an OHG specimen formed at $C_{SF} = 5$ w/v% and $x_{C18A} = 0.30$. G' (filled symbols), G'' (open symbols), and $tan\,\delta$ (lines) are plotted against ω. The data were recorded at 25 °C, after heating to 65 °C, and cooling back to 25 °C. $\gamma_0 = 0.1\%$. b) Images of an OHG specimen in temporary bended shape, and recovery of the permanent road shape during heating from 42 to 54 °C. c) Shape-fixity ratio R_f of OHGs formed at various x_{C18A} contents. $C_{SF} = 5$ w/v%. d) Shape-recovery ratio R_r of OHGs shown as a function of temperature. $C_{SF} = 5$ w/v%; $x_{C18A} = 0.10$ (◆), 0.20 (▼), 0.25 (▲), and 0.30 (●). $C_{SF} = 20$ w/v%; $x_{C18A} = 0.30$ (○).

domains fixing the created bended shape (Figure 5b). To recover the permanent shape, the specimen is again heated above T_m to melt the crystalline domains so that the polymer chains in OHG assume their most probable chain conformation.

The shape-memory function of OHGs is quantified by the bending tests conducted on OHG specimens created at various x_{C18A} and C_{SF}. Figure 5c shows the shape-fixity ratio R_f of OHGs formed at 5 w/v % SF and at various x_{C18A}. R_f is only around 20% at $x_{C18A} = 0.10$ indicating that the crystalline domain in OHG is unable to fix the temporary shape. As x_{C18A} is increased, R_f also increases, and a complete shape-fixity ratio could be obtained at $x_{C18A} = 0.30$. Figure 5d presents the shape-recovery ratio R_r of OHGs as a function of temperature. It is seen that the shape-recovery occurs completely and over a narrow range of temperature when $x_{C18A} > 0.20$. The shape-memory behavior is due to the thermoplastic component of OHG, namely organogel microinclusions acting as switching segments and hence promoting shape-fixing, while the elastic SF hydrogel component drives OHG to revert to its original shape.

In addition to the efficient shape-memory function of OHGs, they also exhibit extraordinary mechanical properties. **Figure 6**a compares the compressive stress-strain curves of an OHG spec-

imen formed at $C_{SF} = 5$ w/v % and $x_{C18A} = 0.30$ with its cryogel and organogel components. The data are presented as the dependence of the nominal stress σ_{nom} (force acting per cross-sectional area of the undeformed specimen) on the strain ϵ (change in the length / initial length of the specimen). The fracture stress σ_f of OHG is ten- and three-times higher than its cryogel and organogel components, respectively, i.e., 30 MPa versus 3 and 10 MPa. Moreover, the inset to Figure 6a reveals that the toughness W of the cryogel and organogel components of OHG is 0.2 and 1.7 MJ m^{-3}, respectively, while it increases to 5.3 MJ m^{-3} after their combination. Figure 6b,c presents the stress-strain curves of OHGs (solid curves) and SF cryogels (dashed curves) at various C18A (b) and SF contents (c). Their mechanical parameters, namely Young's modulus E, fracture stress σ_f, fracture strain ϵ_f, and toughness W are compiled in Figure 6d as functions of x_{C18A} and C_{SF}. The general trend is that the mechanical performances of all OHGs are much higher than those of the starting cryogels. For instance, Young's modulus E of the cryogel with $C_{SF} = 5$ w/v % is 0.04 MPa, while it two-orders of magnitude increases after incorporation of the organogel with $x_{C18A} = 0.30$ (5.9 ± 0.5 MPa). Moreover, fixing x_{C18A} at 0.30 level while increasing C_{SF} from 5 to 20 w/v % further increases E to 17.7 ± 1.2 MPa which is

www.advancedsciencenews.com

[M] Macro-molecular Materials and Engineering
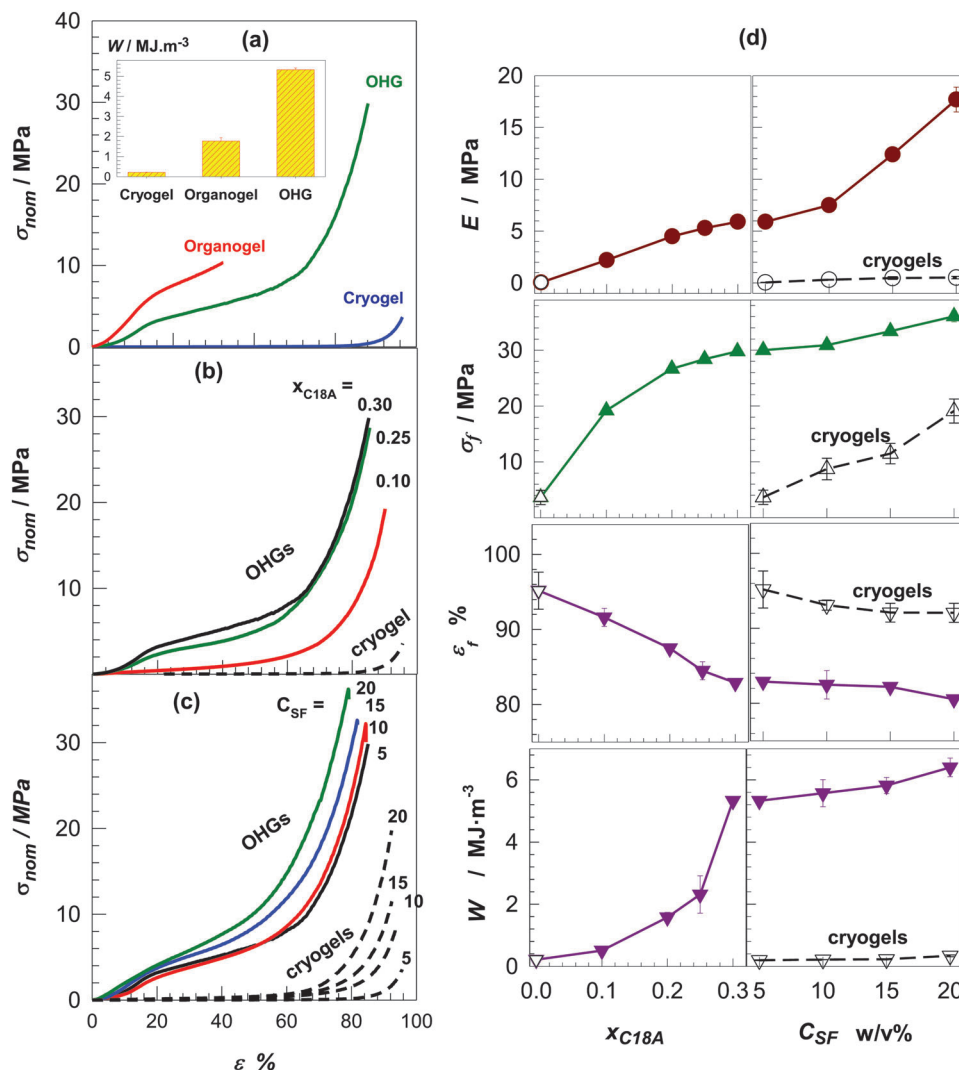Open Access
www.mame-journal.de

Figure 6. a) Stress-strain curves of an OHG specimen formed at C_{SF} = 5 w/v% and x_{C18A} = 0.30, and its cryogel and organogel components. The inset shows the toughness of the OHG and its components. b,c) Stress-strain curves of OHGs (solid curves) and SF cryogels (dashed curves) at various C18A (b) and SF contents (c). d) Young's modulus E, fracture stress σ_f, fracture strain ϵ_f, and toughness W of OHGs plotted against x_{C18A} and C_{SF}. Open symbols represent the data of SF cryogels.

440-fold higher than that of the cryogel. The OHG with the highest modulus E (17.7±1.2 MPa), fracture stress σ_f (36±1 MPa), and toughness W (6.4 ± 0.3 MJ m^{-3}) could be obtained at the highest amount of SF (20 w/v %) and x_{C18A} (0.30). This improvement in the mechanical properties of OHG occurs without changing their thermal properties and shape-memory function (open symbols in Figure 5d). The considerable increase in the mechanical performance of OHGs with increasing C_{SF} is attributed to the decreasing pore size of the cryogels and increasing thickness of the pore walls that surround and protect the brittle organogel microinclusions from damage.[27]

3. Conclusion

We presented mechanically strong OHGs with shape-memory function by incorporating organogel microinclusions within the pores of SF scaffolds. In the first step, SF cryogels with various pore diameters are prepared by cryogelation of aqueous SF solutions of various C_{SF} between 5 and 20 w/v%. The total pore volume of the cryogels decreases from 17 ± 1 to 3 ± 1 mL g^{-1} with increasing SF concentration due to the decreasing amount of ice in the cryogelation system serving as a template for pores. All cryogels exhibit regular micrometer-sized pores with honeycomb morphology. The average pore diameter drops from 26 ± 8 to 17 ± 4 µm as C_{SF} increases from 5 to 20 w/v%. In the second step of OHG preparation, the pores of SF scaffolds are first filled with an organogel precursor solution containing C18A, AAc, BAAm, and AIBN. Once the free-radical polymerization of the organogel precursors took place inside the pores of the cryogels, OHGs containing organo-microgels of various sizes were obtained. The largest amount of organogel can be incorporated in the cryogel scaffold formed at the lowest SF content (5 w/v%), and at the highest C18A mole fraction (x_{C18A}) of 0.30. Moreover, the total pore volume of the initial cryogels significantly decreases after

the formation of OHGs because of the plugging of the pores by the organogels. The incorporation of the organogel component in the cryogels generates crystalline areas due to the side-by-side packed C18 side chains with a spacing distance of 0.41 nm. By adjusting the amounts of C18A and SF, OHG's melting temperature and the crystallinity level could be varied between 42–54 °C, and 2–16%, respectively. The existence of crystalline domains in OHGs resulted in the temperature sensitivity of their viscoelastic properties. For instance, the modulus G' of OHG formed at $C_{SF} = 5$ w/v% and $x_{C18A} = 0.30$ ten-fold decreases upon heating from below to above T_m while cooling back below T_m recovers the original modulus revealing reversible switchable viscoelastic behavior of OHGs. All OHGs with $x_{C18A} > 0.20$ exhibit complete shape-fixity and shape-recovery ratios. The shape-memory behavior is due to the thermoplastic component of OHG, namely organogel microinclusions acting as switching segments and hence promoting shape-fixing, while the elastic SF hydrogel component drives OHG to revert to its original shape. Compared to the cryogel and organogel components, OHGs exhibit much better mechanical properties. For instance, the fracture stress of OHG is 10- and 3-times higher than its cryogel and organogel components, respectively, i.e., 30 MPa versus 3 and 10 MPa. A significant improvement in the mechanical properties of OHGs is also observed with increasing amount of SF during cryogelation. Young's modulus of OHGs increases from 5.9 ± 0.5 to 18 ± 1 MPa with increasing SF concentration from 5 to 20 w/v %. We attribute the considerable increase in the mechanical performance of OHGs with increasing C_{SF} to the decreasing pore size of the cryogels and increasing thickness of the pore walls that surround and protect the brittle organogel microinclusions from damage.

Supporting Information

Supporting Information is available from the Wiley Online Library or from the author.

Acknowledgements

Conflict of Interest

The authors declare no conflict of interest.

Data Availability Statement

The data that support the findings of this study are openly available in the Supporting Information of this article.

[1] J. Huang, R. Fang, T. Zhao, M. Liu, *Polymer* **2020**, *190*, 122214.
[2] J. Mo, S. F. Prévost, L. M. Blowes, M. Egertová, N. J. Terrill, W. Wang, M. R. Elphick, H. S. Gupta, *Proc. Natl. Acad. Sci. USA* **2016**, *113*, E6362.
[3] K. B. Storey, J. M. Storey, *Compr Physiol* **2013**, *3*, 1283.
[4] Y. Xu, Q. Rong, T. Zhao, M. Liu, *Chem. Evol. Giant Planets, [Invited Lect. Colloq.]* **2020**, *2*, 100014.
[5] Z. Zhang, J. Hao, *Adv. Colloid Interface Sci.* **2021**, *292*, 102408.
[6] H. Zhou, J. Lai, B. Zheng, X. Jin, G. Zhao, H. Liu, W. Chen, A. Ma, X. Li, Y. Wu, *Adv. Funct. Mater.* **2021**, *32*, 2108423.
[7] Z. Zhao, C. Li, Z. Dong, Y. Yang, L. Zhang, S. Zhuo, X. Zhou, Y. Xu, L. Jiang, M. Liu, *Adv. Funct. Mater.* **2019**, *29*, 1807858.
[8] Q. Rong, W. Lei, L. Chen, Y. Yin, J. Zhou, M. Liu, *Angew. Chem., Int. Ed.* **2017**, *56*, 14159.
[9] S. Zhuo, Z. Zhao, Z. Xie, Y. Hao, Y. Xu, T. Zhao, H. Li, E. M. Knubben, L. Wen, L. Jiang, M. Liu, *Sci. Adv.* **2020**, *6*, eaax1464.
[10] Q. Ding, Z. Wu, K. Tao, Y. Wei, W. Wang, B.-R. Yang, X. Xie, J. Wu, *Mater. Horiz.* **2022**, *9*, 1356.
[11] C. B. Oral, B. Yetiskin, C. Cil, F. N. Kok, O. Okay, *ACS Appl Bio Mater* **2023**, *6*, 1594.
[12] H. Gao, Z. Zhao, Y. Cai, J. Zhou, W. Hua, L. Chen, L. Wang, J. Zhang, D. Han, M. Liu, L. Jiang, *Nat. Commun.* **2017**, *8*, 15911.
[13] B. Yetiskin, O. Okay, *ACS Appl Polym Mater* **2022**, *4*, 5234.
[14] O. Okay, *Prog. Polym. Sci.* **2000**, *25*, 711.
[15] (Ed.: O. Okay), *Adv. Polym. Sci.*, Springer, Berlin, Germany **2014**, *263*.
[16] O. Okay, V. I. Lozinsky, *Adv. Polym. Sci.* **2014**, *263*, 103.
[17] I. Karakutuk, F. Ak, O. Okay, *Biomacromolecules* **2012**, *13*, 1122.
[18] F. Ak, Z. Oztoprak, I. Karakutuk, O. Okay, *Biomacromolecules* **2013**, *14*, 719.
[19] X. Chen, D. P. Knight, Z. Shao, F. Vollrath, *Biochemistry* **2002**, *41*, 14944.
[20] C. Mo, C. Holland, D. Porter, Z. Shao, F. Vollrath, *Biomacromolecules* **2009**, *10*, 2724.
[21] M. V. Dinu, M. M. Ozmen, E. S. Dragan, O. Okay, *Polymer* **2007**, *48*, 195.
[22] F. M. Plieva, M. Karlsson, M.-R. Aguilar, D. Gomez, S. Mikhalovsky, I. Y. Galaev', *Soft Matter* **2005**, *1*, 303.
[23] H. Kirsebom, G. Rata, D. Topgaard, B. Mattiasson, I. Y. Galaev, *Macromolecules* **2009**, *42*, 5208.
[24] M. M. Ozmen, O. Okay, *J. Macromol. Sci. Part A* **2006**, *43*, 1215.
[25] C. Bilici, V. Can, U. Nöchel, M. Behl, A. Lendlein, O. Okay, *Macromolecules* **2016**, *49*, 7442.
[26] E. Su, C. Bilici, G. Bayazit, S. Ide, O. Okay, *ACS Appl. Mater. Interfaces* **2021**, *13*, 21786.
[27] H. Huang, Z. Dong, X. Ren, B. Jia, G. Li, S. Zhou, X. Zhao, W. Wang, *Nano Res.* **2023**, *16*, 3475.